

Characterisation of VISTA IR detectors

Nagaraja Bezawada^a, Derek Ives^a and Guy Woodhouse^b

^aUK Astronomy Technology Centre, Royal Observatory, Blackford Hill, Edinburgh EH9 3HJ, UK

^bRutherford Appleton Laboratory, Chilton, Didcot OX11 0QX, UK

ABSTRACT

VISTA awarded a contract to Raytheon Vision Systems in June 2002 to supply 16 SWIR HgCdTe 2Kx2K detectors. Raytheon has delivered VIRGO 2K x 2K readout multiplexers, engineering detectors and the first two science grade detectors. The UKATC has set up a low background test facility to test and characterize the VIRGO detectors and to confirm that the detector performance meets our specifications. The VIRGO 2Kx2K is a new detector being produced for VISTA by Raytheon. In this paper we present the first results and performance of the multiplexer and the science detector. The test facility includes a custom built low background close-cycle cooled cryostat, cryogenic pre-amplifier electronics and uses ESO's Infrared array controller electronics and detector control and data acquisition software. The detector parameters being measured include trans-impedance conversion gain, quantum efficiency in J, H and K wave bands, read noise, dark generation rate, linearity, well capacity, pixel operability, drift with temperature, persistence and electrical cross-talk.

Keywords: VIRGO IR detectors, HgCdTe SWIR, characterisation, VIRGO multiplexer, VISTA

1 THE VISTA IR DETECTORS

1.1 VISTA IR detectors

The VISTA IR Camera¹ is a wide-field infrared imager for VISTA² with the world's largest IR focal plane populated with 16 VIRGO infrared 2Kx2K detectors. The camera has a 1.6 degree field of view sampled at 0.34 arc seconds per pixel. VISTA awarded a contract to Raytheon Vision Systems, USA, to supply 16 2K x 2K science grade detectors, 3 bare multiplexers and 4 engineering grade detectors for the IR camera project.

1.2 VIRGO 2Kx2K detectors

The shortwave infrared (SWIR) VIRGO sensor chip assembly (SCA) arrays are p-on-n type HgCdTe IR detectors grown by a liquid phase epitaxy (LPE) process on lattice matched CdZnTe substrates and hybridised to VIRGO silicon readout arrays³. The detector cut-off wavelength has been tuned to 2.5 μ m. The shortwave cut-off wavelength is 0.85 μ m due to the cut-off of the CdZnTe substrate. The detectors are coated with anti-reflection layers optimised for 1.4 μ m for peak reflectivity and have measured quantum efficiencies greater than 90% in certain bands. The pixel size is 20 μ m square and uses a source follower per detector (SFD) in unit cell architecture. Further details on the detector process and performance are reported elsewhere in these proceedings⁴.

1.3 VIRGO readout

VIRGO readout can be organized into vertical strips of either 128 or 512 columns x 2048 rows which are processed through 16 or 4 outputs respectively. The VIRGO design allows up to a maximum of 400 kHz pixel rate which equates to a 0.68s frame readout time in 16 output mode. The first row of the array consists of reference pixels which are held at reset level (starvation) and a row at the top of the array which consists of pixels which are held at saturation. In addition to these reference pixels, there are six other reference pixels in each row in each output of 16 output mode; two pixels before and 4 pixels after the active pixels. The VIRGO detector is designed to be clocked with only two clocks (a master clock and a frame start). All other necessary clocks to operate the row and column shift registers are generated on-chip. Three control lines allow the selection of output mode, reset frame and reset type (global or line-by-line reset). Fifteen different biases are required to operate the detector (some of the biases are used as upper and lower rails for internally generated clocks). The VIRGO detectors are 3-side buttable with all the electrical connections available on one side

through a flex cable terminated with 51-pin micro D-connector. Detector power dissipation is approximately 8mW in its normal operation (1Hz frame rate in 16 output mode).

2 THE TEST SETUP

The UKATC has set up a low background test facility to test and characterise the VIRGO detectors and to confirm that the detector performance meets the specifications. The test facility includes a custom built low background close-cycle cooled cryostat, cryogenic pre-amplifier electronics and ESO's Infrared Array Controller Electronics (IRACE), detector control and data acquisition software. The detector parameters being measured include transimpedance conversion gain, quantum efficiency in J, H and K wavebands, read noise, dark generation rate, linearity, well capacity, pixel operability, drift with temperature, persistence and electrical cross-talk.

2.1 Cryostat

The low background test cryostat includes a detector mount suitable for the VIRGO detector, a manually operated cold filter wheel in front of the detector and a preamplifier fan-out board close to the detector. The detector mount (Fig. 1) contains a temperature controlled stage which can be operated from 50K to 90K. The detector is surrounded by a low background baffle on the detector mount to prevent scattered light reaching the detector. The filter wheel allows the detector to be illuminated through J, H and K filters for quantum efficiency measurements, uniformity measurements and mapping of defect or hot pixels. A cold blank is positioned in front of the detector for estimating dark current generation and image persistence measurements. Located close to the detector mount is a 16-channel differential preamplifier fan-out board. The differential preamplifiers use TLC2274 CMOS op-amps which work reliably at temperatures well below (approximately down to 45K) the detector operating temperature⁵. The differential outputs of each preamp are DC coupled to the IRACE acquisition modules. The bias and clock voltages from the IRACE are further filtered and over-voltage protected with clamping zener diodes in the pre-amp board. The detector mount and the filter wheel assembly are surrounded by a low background radiation shield which is mounted directly on to the cold plate connected to the closed cycle cold head. The cold plate temperature is around 42K during operation.

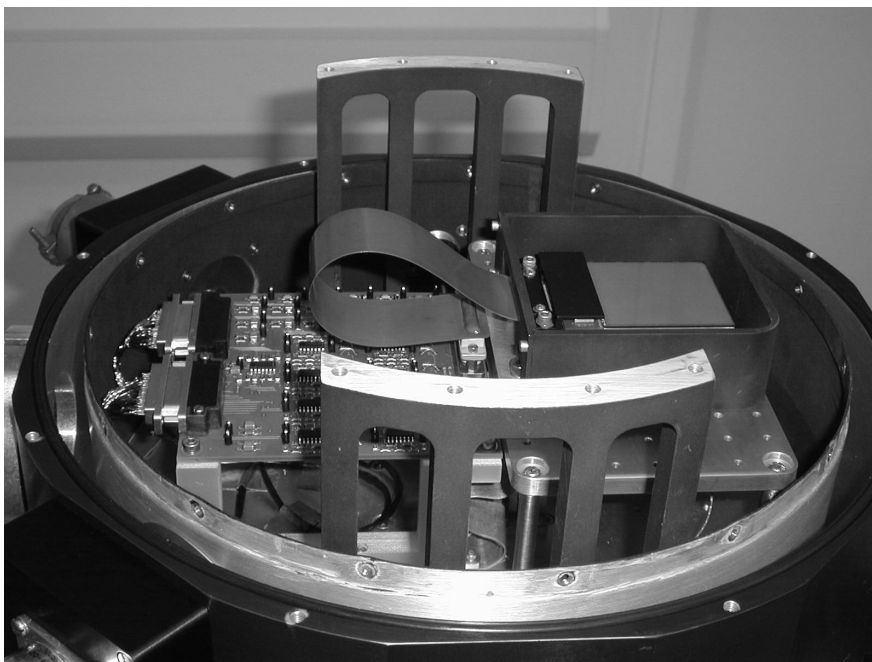


Fig. 1. Detector in its mount and preamplifier board

2.2 IRACE electronics

Infrared Array Controller Electronics (IRACE) developed by ESO⁵ is used to drive the VIRGO-2K detector. The IRACE consists of detector front-end electronics (DFE), detector backend electronics (DBE) and a SUN Ultra-60 data acquisition computer. The DFE and DBE are connected through a high-speed fiber link while the DBE is interfaced through its DMA module to the host computer through a PCI bus DMA card. The data acquisition software allows complete control of the electronics and can be either operated using a GUI based detector control software (DCS) or through a more powerful interactive (stand alone) mode. The system configuration, detector configuration, voltages, clock sub-patterns etc. can be defined by ASCII files. A real time data display captures the incoming data and provides an online display.

2.3 Radiometric setup

An extended area blackbody is used to illuminate the detector and to perform QE measurements. The operating temperature range of the blackbody is 50 - 600°C, settable to 0.1°C resolution using a blackbody temperature controller. The detector is illuminated through a cold aperture (optical pinhole) which is installed inside the cryostat at a known distance from the detector plane to define f-number for estimating the photon flux at the detector plane. The flux incidence on the detector plane at a given blackbody temperature is estimated from Planck's equations⁶. The transmission characteristics of the filters and the window are taken into account for these measurements.

3 VIRGO MULTIPLEXER

3.1 Basic operation

The unit cell in the Readout integrated circuit (ROIC) consists of three transistors which form a source follower per detector (SFD) input circuit (Fig.2). The photo-generated carriers (holes) in the detector cause the voltage on the gate of the source follower to charge from the reset voltage (0V) towards the detector common voltage (0.5V). In a bare multiplexer, the electron-hole pairs are separated by the p-n junction formed by the n-type diffusion of the n-channel reset FET. Thus the bare multiplexer integrates towards negative while with the IR detector material (p-on-n), the SCA integrates positive from the reset level. When a row is addressed (row enable), all the source followers in that row are connected to their own 'idle' current source at the end of each column. A 'slew' current source is connected to the column bus, one pixel period prior to multiplexing the selected column to the output source follower, to allow the unit cell source follower to drive the capacitance of the common output bus.

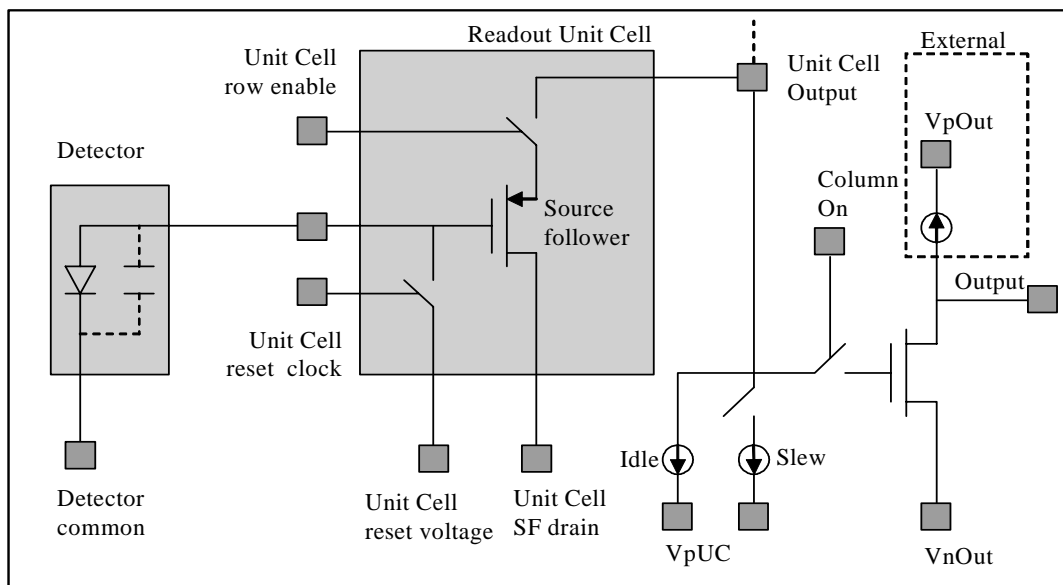


Fig. 2. Detector and unit cell construction

3.2 Cold test results

The VIRGO multiplexer has been cooled to 72K and operated at about 280kHz pixel rate. Table 1 lists the performance parameters for the cold operation.

Table 1. Performance summary

Parameter	Value
Conversion gain ($\mu\text{V}/e^-$)	7.79
Full well (ke^-)	~80
Output DC level (V)	3.45
Non-linearity (%)	3.25
Read noise (e^-)	9.2
SF gain	0.97

The system gain (e/ADU) is found using the well known photon transfer technique. The detector transimpedance conversion gain ($\mu\text{V}/e^-$) is then obtained with the knowledge of the preamplifier gain and the ADC transfer function. The DC output level is obtained from an un-correlated dark frame with minimum detector integration time (1sec at 1Hz frame rate). The source follower gain is obtained by plotting the DC output against varying 'VReset' whilst the array is kept under continuous reset.

3.3 Row reset

The VIRGO detector clocking scheme is shown in Fig. 3. After receiving a frame start pulse, the pixels are sequentially accessed at every rising and falling edge of the master clock. A row can be reset (if reset is enabled) after accessing the pixels in that row. In other words, the reset takes place at the end of each row during one master clock period. During multiplexer cold testing, it was found that the reset time was just sufficient at 200kHz pixel rate ($10\mu\text{s}$ reset time) but insufficient at 400kHz and needed slightly longer reset time for complete resetting of the row. This is achieved by freezing the master clock during reset as long as necessary to allow longer rest time. Since the CMOS logic is entirely static and driven by master clock, this change in the period of the master clock causes no problem.

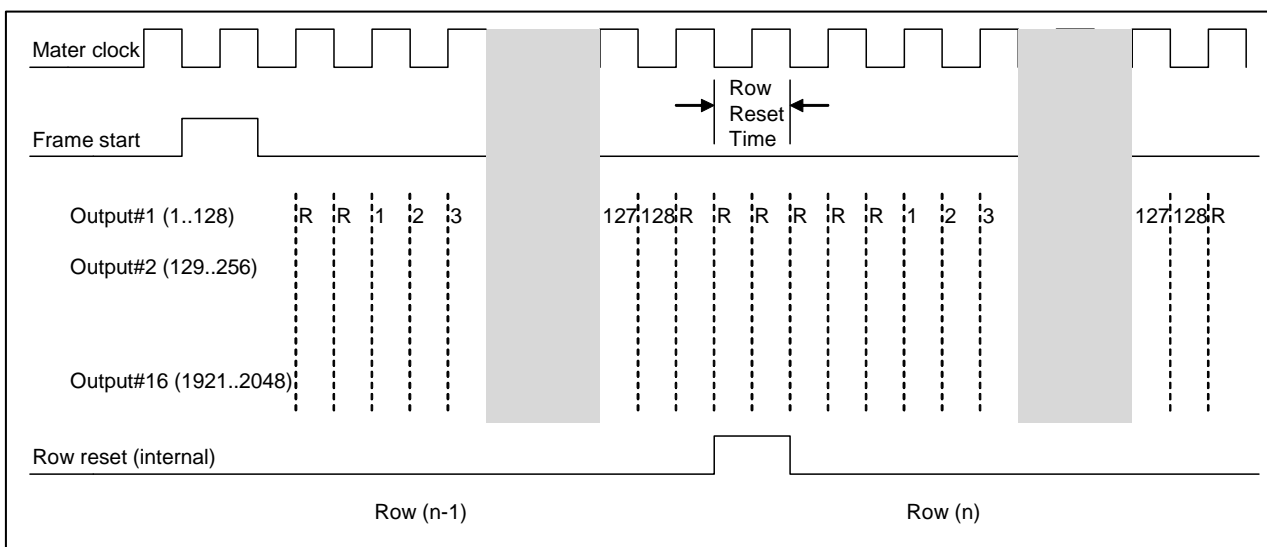


Fig. 3. VIRGO multiplexer clocking scheme

3.4 DC uniformity

The DC uniformity frame is obtained from a dark uncorrelated frame with minimum detector integration time (1s). A sequence of 10 such frames is averaged to reduce the read noise. The DC uniformity frame and its histogram are shown

in figures 4 and 5 for multiplexer VM301-004. The multiplexer is operated at about 294kHz pixel rate (each channel) with frame readout time of 1.001sec including the extra delay for a complete row reset. A pixel reset voltage (VrstUc) of 0.0V is used for these tests. The standard deviation in offset uniformity is about 15mV and the operability is 99.9% of pixels within 5-sigma. The mean source follower gain is 0.974 with <0.5% non-uniformity (sigma/mean).

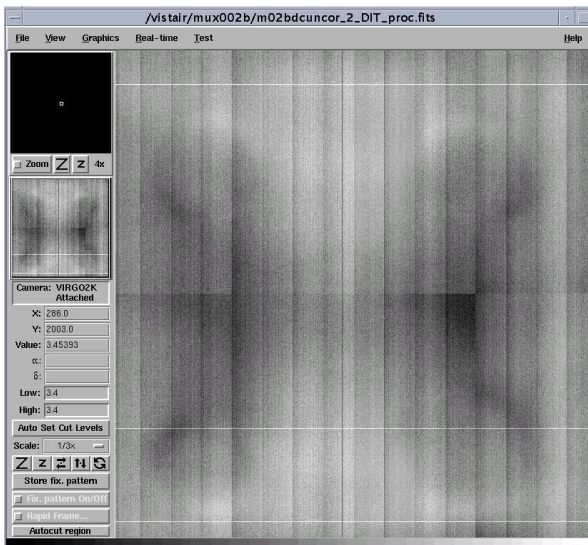


Fig. 4. DC uniformity of cold multiplexer

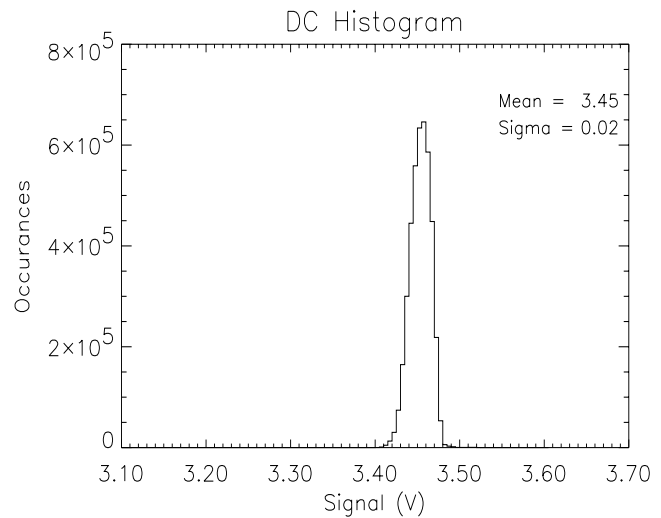


Fig. 5. DC uniformity histogram (Mean DC = 3.45V)

4 SCIENCE DETECTORS

Raytheon have now delivered the first two science detectors, SCA-22 and SCA-24. The SCA-22 has been operated at 294 kHz pixel rate in each channel, with 16 output channels allowing a frame readout time of 1 sec. A row-by-row reset is used for resetting the detector. The following sections describe the performance of the SCA-22 science detector.

4.1 Transimpedance conversion gain

As before, the system gain is determined from photon transfer technique using several pairs of identical flats with signal values ranging from just above bias level to saturation by varying the integration time whilst the input flux is kept constant. The gain is determined from the histogram method for better accuracy using the following equation:

$$\text{SystemGain} = \frac{\text{Signal(ADU)}}{\text{SignalNoise(ADU)}^2 - \text{ReadNoise(ADU)}^2}$$

The read noise in the above equation is the pixel-to-pixel read noise. The gain is estimated from a number of small regions within the array and a histogram of the gain data is plotted. The mean of the gain histogram is the system gain in e^-/ADU . Fig. 6 shows the system gain computed from signal levels from 20% to 70% of full well. The system gain of $6.076e^-/\text{ADU}$ translates to transimpedance conversion gain of $3.75\mu\text{V}/e^-$ and corresponds to a detector node capacitance of 40fF (at 0.7V detector bias) which is close to the model predicted value. It has been observed that the system gain (hence, the transimpedance conversion gain) varies with increasing signal level. Fig. 7 shows that this gain variation with signal level is up to 18%. This is caused by the fact that the detector junction capacitance increases as the input node integrates towards saturation and hence the conversion gain ($\mu\text{V}/e^-$) decreases.

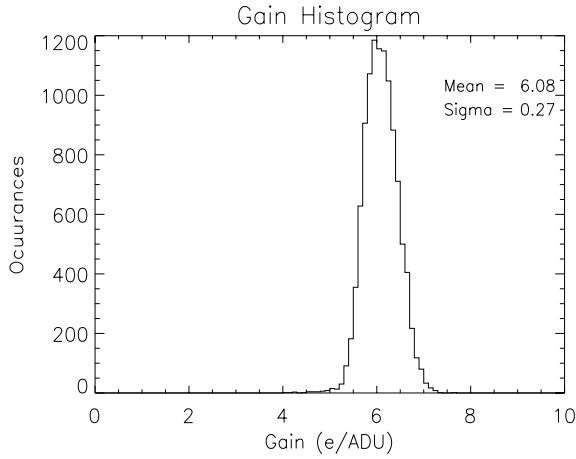


Fig. 6. System gain determination

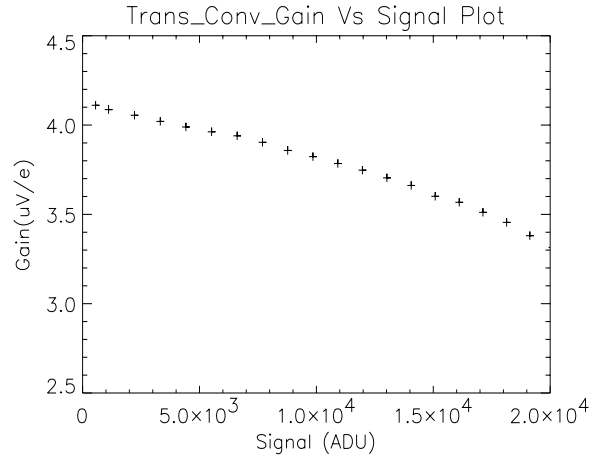


Fig. 7. Gain variation with signal level

4.2 Full well and non-linearity

The full well capacity is determined from the noise rollover point in the variance vs. signal plot (Fig. 8). The full well capacity is dependent on the detector capacitance (C_{det}) and the applied detector bias (Det. bias) as given by:

$$\text{Fullwell}(e^-) = \frac{C_{det} * \text{Det.bias}}{q} \quad \text{where } q = 1.602 \times 10^{-19} \text{ Coulombs}$$

The detector bias also slightly alters the detector pixel capacitance and hence the conversion gain changes. The detector bias is given by $V_{Reset} - V_{detCom}$ and thus can be varied by either of these voltages. The V_{detCom} is varied while V_{rstUC} is fixed at 0.0V to set different detector biases. The higher V_{rstUC} gives higher DC output level which is not advantageous in our system because we have quite low supply rails in the signal processing chain. Non-linearity is derived from a plot of output signal vs. integration time. A least squares fit is fitted to the data from 10% to 80% of the full well. The non-linearity is obtained from the following equation:

$$\text{Non-linearity}(\%) = \left(\frac{\text{MeasuredData}}{\text{FitData}} - 1 \right) * 100$$

Fig. 9 shows the non-linearity of 5.1% (p-v) for a detector bias of 0.7V. Table 2 gives summary of the well capacity, non-linearity, transimpedance conversion gain and dark generation at different detector bias levels.

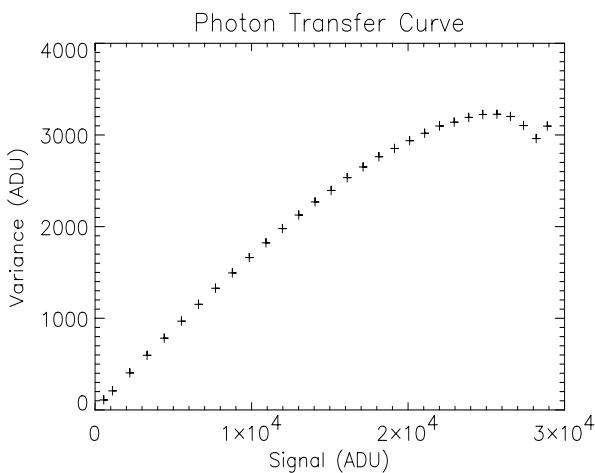


Fig. 8. Full well capacity from photon transfer (0.7V det. bias)

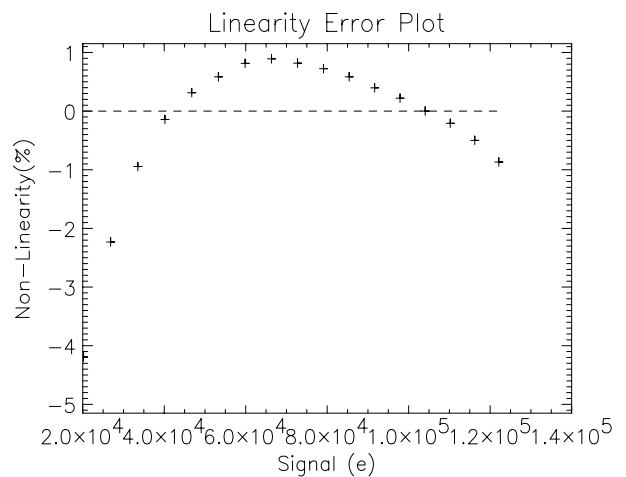


Fig. 9. Non-linearity (10 – 80% of full well)

Table 2. Summary of parameters at different detector bias levels

Parameter (72K)	0.5V Bias	0.6V Bias	0.7V Bias
Conversion gain ($\mu\text{V}/e^-$)	3.58	3.68	3.75
Full well (ke^-)	102	131	156
Non-linearity (p-v, %)	3.2	-	5.1
Dark generation (e^-/s)	1.7	1.9	2.0

4.3 Dark generation

A series of dark frames are obtained each with 240s integration time and an average dark frame is generated. The frame is then converted into electrons/s (Fig. 10) and a histogram (Fig. 11) is generated. The mean of the histogram shows the average dark generation of $1.76e^-/s$ at 72K. The mean dark generation in the central region is about $1.3e^-/s$ at 72K.

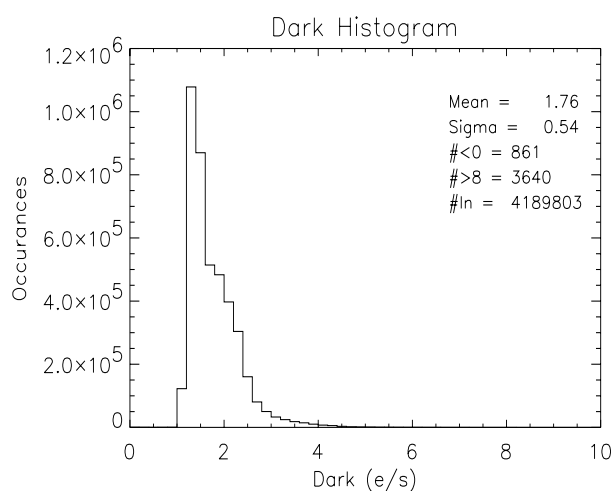
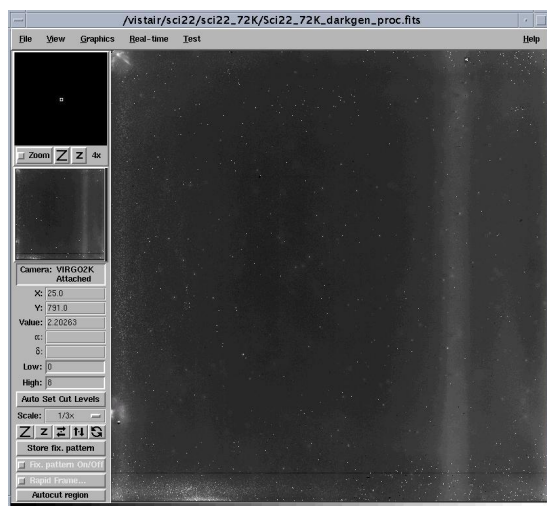


Fig. 10. Bitmap of dark generation (stretched between 0 - 8e/s) Fig. 11. Histogram of dark generation (72K)

4.4 Quantum efficiency

The quantum efficiency of the detector is measured in J, H and K pass bands using blackbody radiometry. The flux incidence on the detector plane at a given blackbody temperature is estimated from Planck's law. The transmission characteristics of the filters and the window and flux attenuation due to cold aperture are taken into account for these measurements. The detector QE and uniformity are determined at 65K, 72K and 77K operating temperature. Detector cosmetics and uniformity tend to improve (see section 4.7) at lower temperatures whilst absolute QE tends to reduce (Table 3). The uncertainty values estimated for the test cryostat are up to 12% and are mainly due to the uncertainties in the temperature of the blackbody, emissivity of the blackbody and spectral band-pass transmission. The actual uncertainties may be bigger due to unwanted reflections and light scattering within the test cryostat. Fig. 12 and Fig. 13 show the QE bitmap in K-band and the QE histogram for detector SCA-22. The first light filters of the IR camera will have Ks instead of K filter.

Table 3. QE and dark generation dependency on operating temperature

Parameter	Value(65K)	Value(72K)	Value(77K)
Conversion gain ($\mu\text{V}/e^-$)	-	3.58	3.61
Dark Generation (e^-/s)	1.4	1.7	2.7
QE - J (%)	67.8	71.1	73.2
QE - H (%)	71.9	75.0	77.0
QE - K (%)	72.3	75.0	76.7

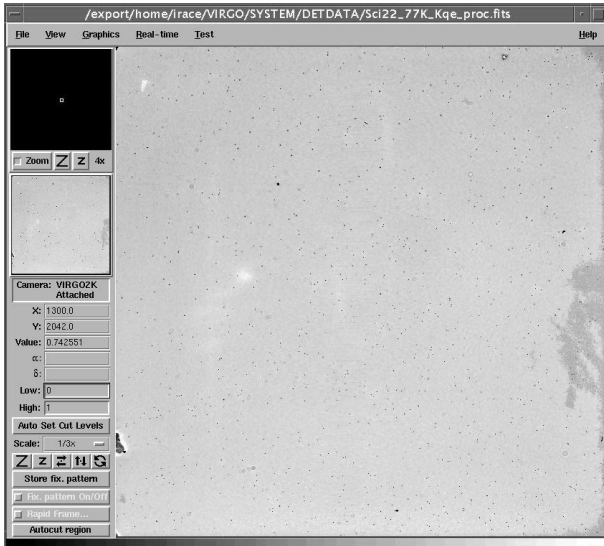


Fig. 12. QE bitmap in K band (2.06 μ m – 2.43 μ m).

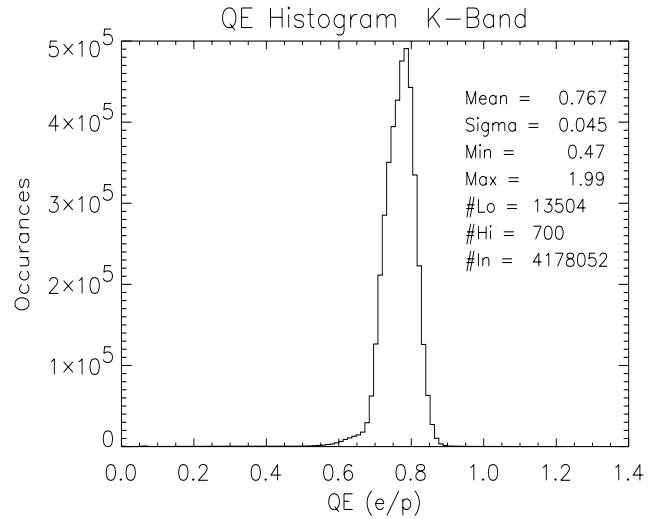


Fig. 13. QE histogram in K band – operability > 99.6%

4.5 Read noise

Two methods for measuring read noise are used. The temporal noise method involves collecting a series of CDS dark frames obtained with minimum detector integration time. A noise frame (in ADU) is generated by measuring noise in every pixel from all the dark frames on a pixel-by-pixel basis. The resultant noise frame is converted into electrons by multiplying with the system gain and a histogram is generated. The mean of the histogram is the temporal read noise. The pixel-to-pixel read noise is measured from only two CDS dark frames with minimum detector integration time. The two frames are subtracted from each other. The standard deviation estimated from a region free of defects in the resulting frame divided by $\sqrt{2}$, is the pixel to pixel read noise in a CDS frame. A close agreement between the two methods is obtained. Fig. 14 shows the temporal noise bitmap. Mean read noise of 17.3e⁻ (Fig. 15) is obtained from active pixels while it is $\sim 10e^-$ for the reference pixels.

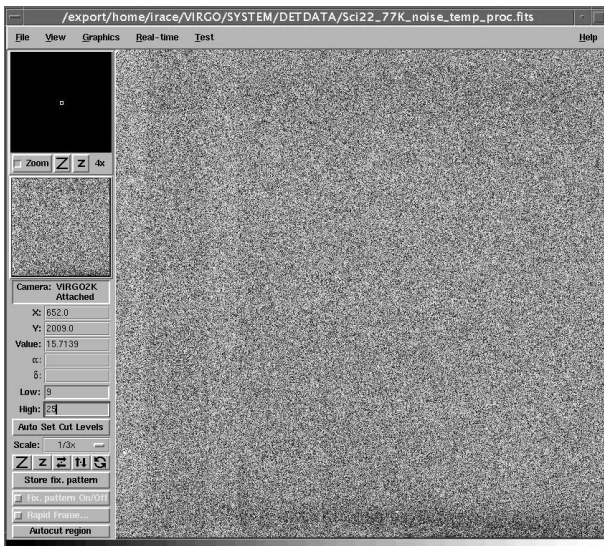


Fig. 14. Temporal read noise bitmap (full frame)

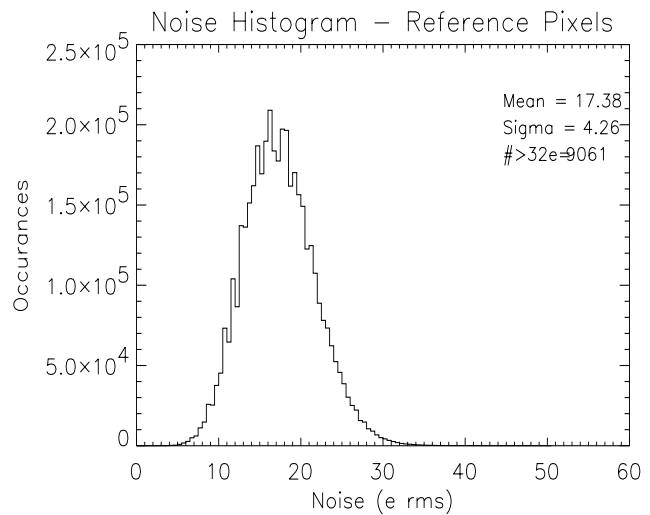


Fig. 15. Read noise histogram

4.6 Persistence

A few pixels are exposed through an adjustable aperture close to the blackbody to produce a spot with FWHM of about 20 pixels. The detector is saturated with roughly 200ke^- fluence (10sec exposure). Soon after the exposure, the cold blank is positioned in front of the detector and a sequence of 10sec integrated dark frames is investigated for persistence signal decay. The persistence signal is dependent on the fluence, source flux and delay after exposure. Fig.16 shows a series of images of the remnant signal in subsequent 10 sec dark exposures. As seen from Fig. 17, the persistence signal in a 10sec. dark exposure, after saturating the detector with about 200ke^- fluence, decays down to read noise level in about 40 sec after the first array reset.

The effect of number of resets on the persistence signal is also investigated. The remnant signal in 2nd 10sec dark frame with 1 reset (Fig. 17) is the same as the remnant signal in the first 10 sec dark frame with 10 resets (Fig. 18). Since a reset takes 1s (same as read array), it is the time that the persistence signal has to decay after the first array reset that is important. The number of resets had no or little effect on the persistence signal.

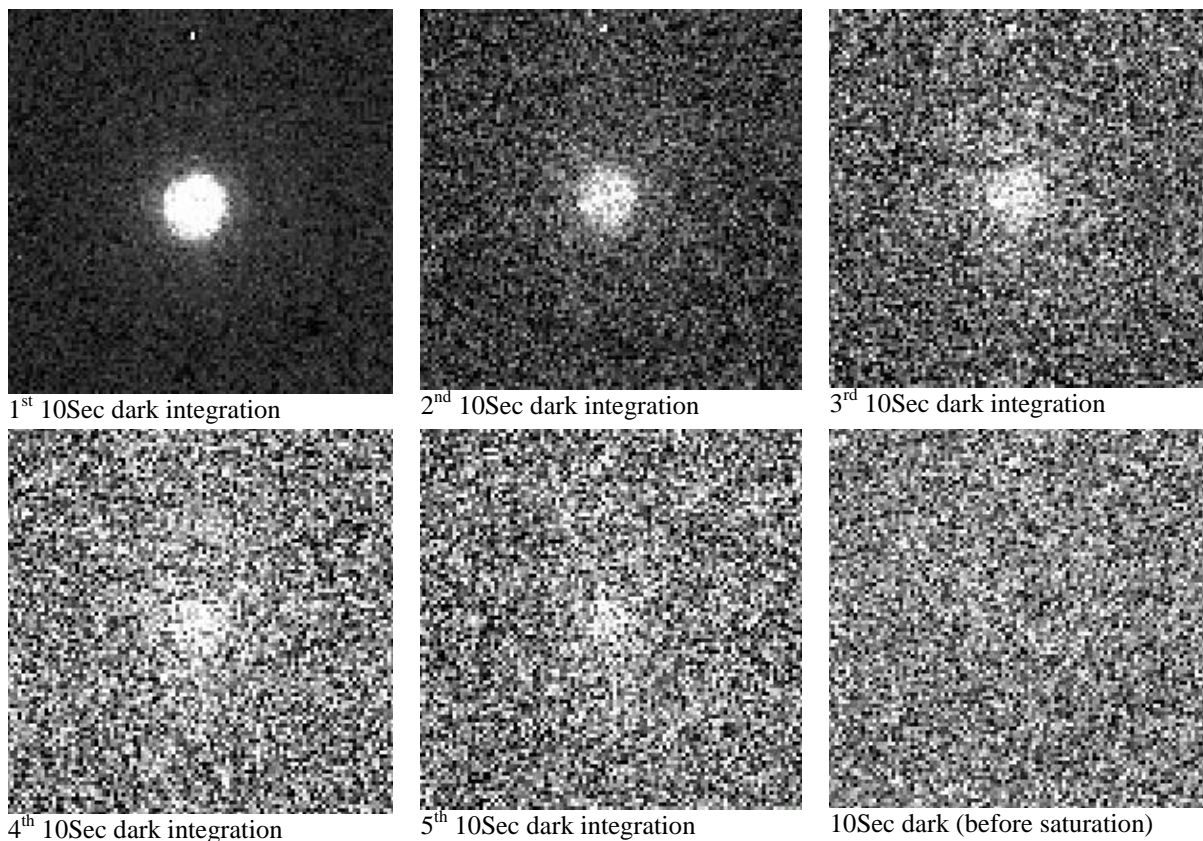


Fig.16. Persistence signal decay

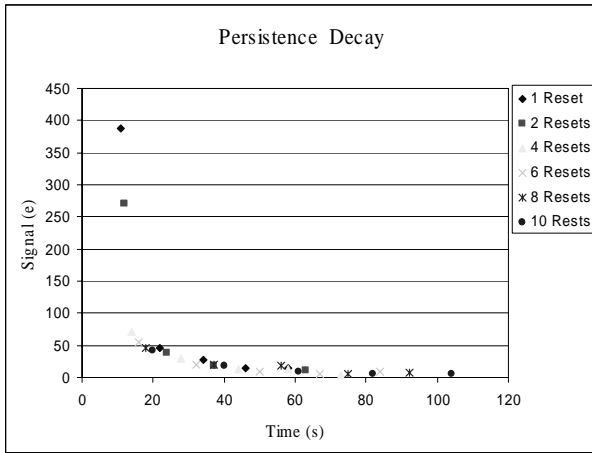


Fig. 17. Persistence decay in subsequent frames of 10s

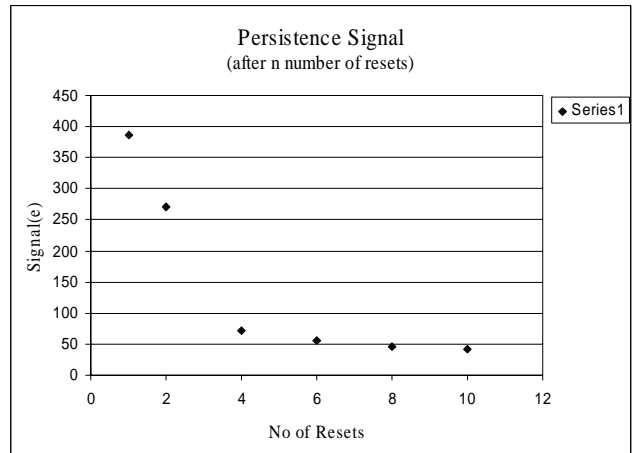


Fig. 18. Persistence signal in first 10s frame after n resets

4.7 DC drift

The mean output DC level varies with the detector operating temperature. Several dark uncorrelated frames with minimum detector integration are obtained at three different operating temperatures (77K, 72K and 65K). The data is converted into voltage at the detector output. The slope of the plot with detector output voltage vs. the operating temperature gives the detector output drift with temperature (Fig. 19). A drift of 3mV/K is measured for SCA-22 which is equivalent to $838e^-/K$. Both reference and active pixels show similar drift with temperature.

4.8 Pixel operability

The pixel operability is obtained from QE and hot pixel maps. A pixel is defined as inoperable if its QE is less than the requirement or its dark generation greater than requirement. The data used to estimate the dark generation is used to generate a map of pixels whose dark is greater than 8e/s and less than 0e/s. From the QE frames in each band, a map of pixels whose QE is less than the minimum requirement in that band is generated. The inoperable pixel bitmap is then created from the dark defects and QE defects frame. Fig. 20 shows the inoperable pixel bitmap for the SCA-22 module.

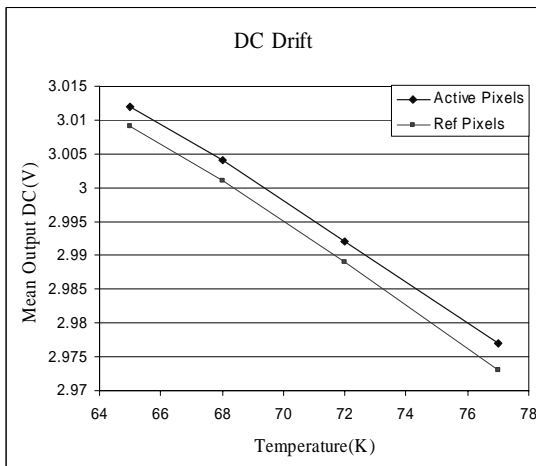


Fig. 19. Measured DC drift for active and reference pixels

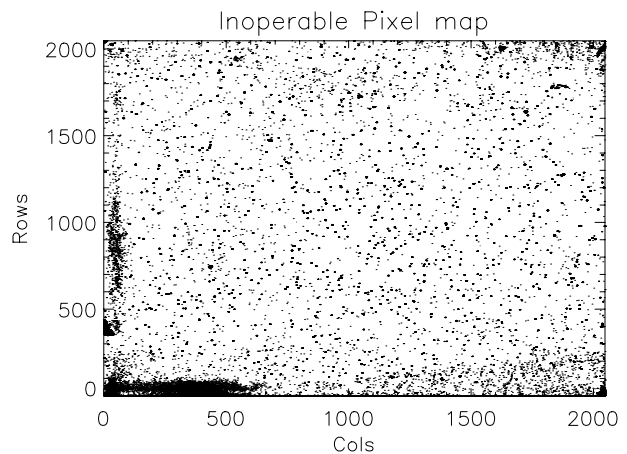


Fig. 20. Inoperable pixel bitmap for SCA-22 (Total pixels inoperable = 0.823%)

4.9 Pixel connectivity

The pixel connectivity is obtained from two uncorrelated frames obtained at two different VdetCom. The open pixels and the reference pixels do not show any shift in the DC level with VdetCom. A map of pixels whose DC level has not been shifted is generated from a resultant frame obtained by subtracting the two uncorrelated frames. This test is performed every time the detector is thermal cycled. The first science module has undergone two thermal cycles at ATC and the open pixels have increased from 190 in first cool down to 239 in the second cool down.

4.10 Detector cosmetics

There are two distinguishing features of the SCA-22 in terms of its cosmetic performance, the defective spots and localized glow centers. The detector has defect spots which are located randomly and uniformly all over the detector. A section of a flat-field (Fig. 21) shows the nature of such spots. The spots are centered on a low responsive pixel typically surrounded by 5 to 7 pixels diameter which show increasing response towards normal pixels. The responsivity of these pixels has the same dependency with temperature as the normal pixels as shown in Table 3. The glow spots are observed in long dark integrations and these are also random in nature, centered on a hot glowing pixel as shown in Fig. 22. The intensity profile of these spots doesn't show much dependency on the operating temperature range from 77K – 65K. Note these features may be specific to this module and are expected to improve in the future modules.

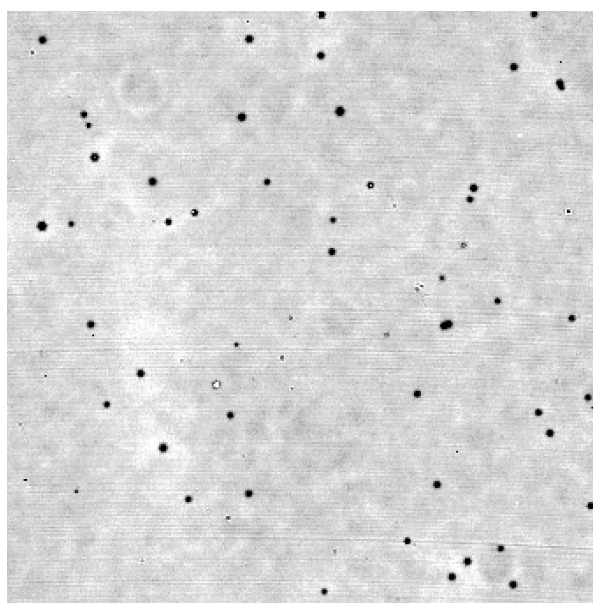


Fig. 21. Defect spots

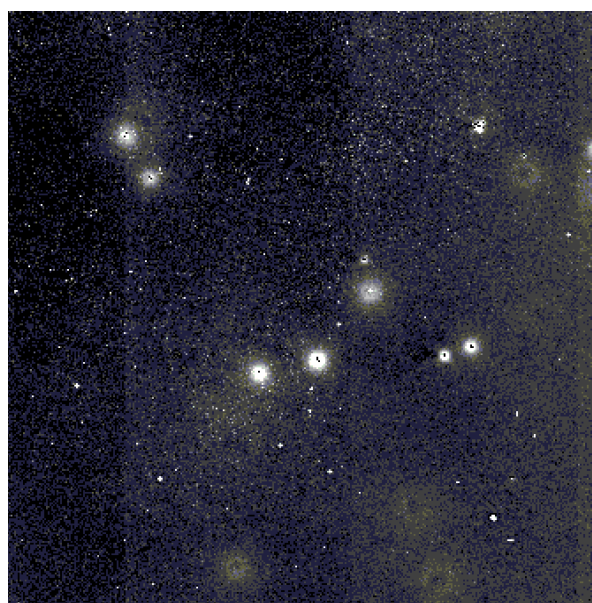


Fig. 22. Localized glow spots in a 240s dark frame

5 PERFORMANCE SUMMARY AND CONCLUSIONS

The first science grade detector meets the requirements with sufficient margin and the overall performance is very good. Full well capacity $\sim 100ke^-$ is obtained at a detector bias of 0.5V with non-linearity slightly above the specification. Full well above $150ke^-$ is achieved with 0.7V detector bias with only a marginal increase in the dark generation. However the non-linearity becomes more pronounced at 0.7V detector bias. An overall operability of $>99\%$ is obtained. Reasonably high QE in all bands with excellent uniformity (non-uniformity $< 7\%$) are obtained with SCA-22. From the persistence measurement, no electrical cross-talk or ghost images of the saturated spot in the other readouts are observed. Table 4 summarizes the performance of the SCA-22 module. Flatness measurements are not measured at ATC, but are reported (from Raytheon's measurements) here for completeness.

Table 4. VISTA IR detectors requirements and results obtained from first science detector.

Parameter	VISTA Requirements	Science detector VM301-SCA-22 (72K)
Format	2048 x 2048	2048 x 2048
Pixel size	15.5 μ m to 20.5 μ m	20 μ m
Wavelength of operation	1.0 μ m to 2.5 μ m	0.85 μ m to 2.5 μ m
Quantum efficiency	> 38% (J) > 47% (H) > 47% (Ks)	71% (J) 74% (H) 75% (Ks)
Well depth	>100ke ⁻	156ke ⁻ (0.7V bias)
Dark generation	<8 e ⁻ /pix/sec	1.7e ⁻ /pix/sec
Read noise	<32 e ⁻ (rms)	17 e ⁻ (rms)
No. of outputs	< 1sec frame rate	16 outputs (1.001s)
Non-linearity	<3%	3.3% (100ke ⁻ FW)
Pixel defects	<4%	<1%
Flatness	< 25 μ m (for FPA)	~6 μ m (p-v)
Conversion gain	-	3.58 μ V/e ⁻
Output DC level	-	3.23V
Operability (%)	-	99.18%

ACKNOWLEDGEMENTS

Many thanks to the Astronomy team at Raytheon Vision Systems for their work for producing the detectors for the VISTA starting from bare multiplexer to the present production of science grade detectors. We thank them for their continued technical support during testing of these detectors. The VISTA IR team gratefully acknowledges help and advice received from Gert Finger, Leander Merghan and Joerg Stegmeier, at ESO with the IRACE. We also thank Kirby Hant and Ron Dewitt of Infrared Laboratories for the custom design and fabrication of the cryostat.

VISTA is funded by a grant from the UK Joint Infrastructure Fund, supported by the Office of Science and Technology and the Higher Education Funding Council for England, to Queen Mary University of London on behalf of the 18 University members of the VISTA Consortium of: Queen Mary University of London; Queen's University of Belfast; University of Birmingham; University of Cambridge; Cardiff University; University of Central Lancashire; University of Durham; University of Edinburgh; University of Hertfordshire; Keele University; Leicester University; Liverpool John Moores University; University of Nottingham; University of Oxford; University of St Andrews; University of Southampton; University of Sussex; and University College London.

REFERENCES

1. G. Dalton, M. Caldwell, K. Ward., M. Whalley, K. Burke, J. Lucas, T. Richards, M. Ferlet, R. Edeson, D. Tye, M. Strachan, E. Atad-Ettegui., M. Leclerc, A. Gallie, N. Bezawada, P. Clark, N. Bissonauth, P. Luke, N. Dipper, P. Berry, W.J. Sutherland, and J.P. Emerson, "The VISTA IR camera", SPIE Vol. **5492**-34, 2004.
2. A.M. McPherson, A.J. Born, and W.J. Sutherland, J.P. Emerson, "The VISTA project: a review of its progress and lessons learned developing the current programme", SPIE Vol. **5489**-46, 2004
3. D.J. Gulbransen, P. J. Love, M. P. Murray, N. A. Lum, C. L. Fletcher, E. Corrales, R. E. Mills, A. W. Hoffman and K. J. Ando, "Megapixel and Larger Readouts and FPAs for Visible and Infrared Astronomy", SPIE Vol. **4841**, pp. 770 – 781, 2003.
4. P. J. Love, A. W. Hoffman, K. J. Ando, D. J. Gulbransen, E. Corrales, N. J. Therrien, J. P. Rosbeck, W. D. Ritchie, R. S. Holcombe, "2K x 2K HgCdTe detector arrays for VISTA and other applications", These proceedings, **5499**-08.
5. M. Mayer, G. Finger, H. Mehrgan, G. Nicolini and J. Stegmeier, "The ESO Infrared Detector High Speed Array control and Processing Electronic IRACE", SPIE Vol. **3354**, pp134-138, 1998.
6. J. D. Vincent, Fundamentals of infrared detector operation and testing, Wiley-Interscience, 1989.